ACS APPLIED MATERIALS & INTERFACES

Research Article

www.acsami.org

Ultrafast Carrier Trapping of a Metal-Doped Titanium Dioxide Semiconductor Revealed by Femtosecond Transient Absorption Spectroscopy

Jingya Sun,[†] Yang Yang,[‡] Jafar I. Khan,[†] Erkki Alarousu,[†] Zaibing Guo,[‡] Xixiang Zhang,[‡] Qiang Zhang,[‡] and Omar F. Mohammed*,[†]

[†]Solar and Photovoltaics Engineering Research Center, Division of Physical Sciences and Engineering and [‡]Advanced Nanofabrication and Imaging Core Lab, King Abdullah University of Science and Technology, Thuwal 23955-6900, Saudi Arabia

ABSTRACT: We explored for the first time the ultrafast carrier trapping of a metal-doped titanium dioxide (TiO_2) semiconductor using broad-band transient absorption (TA) spectroscopy with 120 fs temporal resolution. Titanium dioxide was successfully doped layer-by-layer with two metal ions, namely tungsten and cobalt. The time-resolved data demonstrate clearly that the carrier trapping time decreases progressively as the doping concentration increases. A global-fitting procedure for the carrier trapping suggests the appearance of two time components: a fast one that is directly associated with carrier trapping to the defect state in the vicinity of the conduction band and a slow one that is attributed to carrier trapping to the deep-level state from the conduction band. With a relatively long doping deposition time on the order of 30 s, a carrier lifetime of about 1 ps is obtained. To confirm that the measured ultrafast carrier dynamics are associated with electron trapping by metal doping, we explored the carrier dynamics of undoped TiO_2. The findings reported here may be useful for the implementation of high-speed optoelectronic applications and fast switching devices.

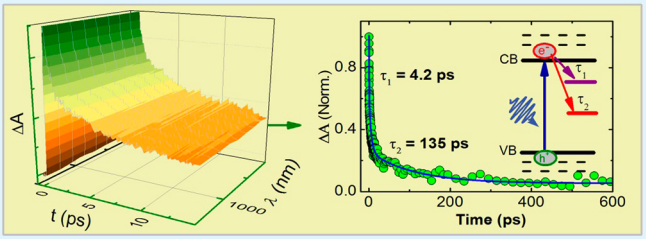

KEYWORDS: *ultrafast carrier trapping, titanium dioxide, transient absorption spectroscopy, metal-doped, deep-level state*

INTRODUCTION

Semiconductor TiO_2 is a widely studied material[1−7] because of its chemical stability, nontoxic nature, inexpensive fabrication, and abundance in nature.[8] This highly versatile material has found many applications in a variety of research areas of significance, including electronics,[9] photovoltaics,[10] photocatalysis,[3] and photoelectrochemical conversion.[11−13] A prominent example is the use of the photocatalytic properties derived from TiO_2[1,14] in the formation of photogenerated charge carriers (electron−hole pairs), which occur with the absorption of ultraviolet (UV) light. In addition, TiO_2 is classified as a unique photocatalyst under light doping in both the visible and UV regions.[4,9,15] It is, in fact, true that the long carrier lifetimes of undoped TiO_2 prevent its use in other potential applications, such as high-frequency switching devices and photodetectors, which mainly rely on very fast carrier recombination as a recovery process to the initial state. In this regard, doping of TiO_2 using metal agents is quite beneficial, as is evidenced in new localized electronic energy levels, defect levels, and a deep-level trap state, induced in the band gap.[6,16] Essentially, an electron is successfully excited from the valence band (VB) to the conduction band (CB) followed by trapping to the generated defect states. Accordingly, in this regime, it is well documented that deep-level states within the band gap can significantly reduce the carrier lifetime. Thus, efforts have been devoted to making these materials suitable for unique applications, including repetitive ultrafast electrical transients and high-speed electronics.[17,18]

Gathering detailed information on intrinsic carrier recombination dynamics due to the metallic dopants in TiO_2 is important. Quantitative data on these carrier dynamics can be directly obtained through ultrafast pump−probe spectroscopy. As a consequence of the action of the pump pulse, electrons are successfully promoted to the CB and subsequently the decay process from the latter band to various defect levels can be directly probed in real time. To achieve this, transient absorption (TA) spectroscopy is a highly sensitive, broad-band, and powerful tool that allows the exploration of ultrafast carrier dynamics in semiconductor materials and complex molecular systems.[16,19−23] For instance, ultrafast carrier dynamics have been thoroughly investigated in numerous semiconductor materials by implementation of this technique, including $SrTiO_3$,[6,24] ZnO,[25] and ZrO_2.[26] In this paper, we report the results from unambiguous, time-resolved experiments on carrier trapping in metal-doped TiO_2 as a function of the deposition time of two metals, tungsten (W) and cobalt (Co). We clearly show that the carrier recombination time decreases dramatically as the metal deposition time increases. Two time constants for

Received: December 27, 2013
Accepted: June 11, 2014
Published: June 11, 2014

carrier trapping are observed: a fast component with a characteristic time constant of a few picoseconds associated with the trapped carriers near the CB and a slow component of a hundred picoseconds attributed to the trapped carriers in the deep-level state.

EXPERIMENTAL SECTION

In this section, we outline the experimental scheme, which includes the synthesis method of the materials and the ultrafast femtosecond transient absorption (fs-TA) spectroscopy technique.

TiO_2−M−TiO_2 (M = W and Co) Multilayer Film Synthesis. The procedure for the sample preparation was previously reported in detail.[27] We provide a brief description with the particular samples used in this work. TiO_2−M−TiO_2 (M = W and Co) multilayer films were deposited on glass substrates using radio-frequency reactive magnetron sputtering. For each sample, four layers of TiO_2 and three layers of the selected metal were deposited. Alternately, one layer of TiO_2 and one layer of the metal were deposited as this procedure was repeated three times. After the TiO_2/metal layers were deposited, an additional layer of TiO_2 was added as a cover. The total thickness of the TiO_2 layers was about 80 nm. The deposition rates of the W and Co layers were 10 and 5.3 nm/min, respectively, and two different deposition times of 10 and 30 s were selected. After deposition, all TiO_2−M−TiO_2 films were annealed at 500 °C in air for 2 h.

Transmission electron microscopy (TEM) cross-sectional specimens were prepared using the focused-ion-beam technique on a FEI Helios 400S to identify the structure of the TiO_2 films and the concentration of the metal dopants. The TEM and scanning transmission electron microscopy (STEM) images were obtained using a FEI Titan 80-300 SuperTwin electron microscope, operated at 300 kV. To analyze the state of the dopant agents and clarify the distribution within the multilayer thin films, electron energy-loss spectroscopy (EELS) was performed on a Gatan Imaging Filter Tridiem.

fs-TA Spectroscopy. Ultrafast time-resolved TA spectroscopy[28,29] was used to study the carrier trapping. An Ultrafast Systems (Sarasota, FL) Helios UV−near-infrared (NIR) system was used to explore the semiconductor samples in this study by employing a pump−probe technique. The Helios system is equipped with CMOS vis (visible) and fast InGaAs NIR spectrometers covering the wavelength range of 350−800 nm with 1.5 nm spectral resolution at 9500 spectra/s and a range of 800−1600 nm with 3.5 nm spectral resolution at 7900 spectra/s, respectively.

The output pulse from the laser system is split into two parts to generate the pump and probe pulses. A small portion (≈60 μJ) of the Spitfire (Spectra-Physics Pro 35F-XP regenerative femtosecond amplifier) output is routed via a delay line, adjustable pinholes, a focusing lens, and a variable neutral density filter to a crystal for white-light-continuum (WLC) generation and further to the sample via a focusing mirror. Three crystals are available to cover the UV−vis and NIR spectra. A computer-controlled delay line is used to vary the time delay between the pump and probe pulses that allow for TA measurements within a 3.3 ns time window. For UV−vis WLC generation, we used a CaF_2 crystal and a sapphire plate for 340−700 and 440−830 nm spectral ranges, respectively. Another part (1 mJ) of the Spitfire output is used to pump a TOPAS-C (Spectra-Physics, Santa Clara, CA) two-stage parametric amplifier equipped with frequency mixing stages and a noncollinear difference frequency generator that allows for tuning from 237 to 2700 nm. The TOPAS-C output beam is routed via the adjustable pinholes, a variable neutral density filter, a depolarizer, a chopper wheel, and a focusing lens to excite the sample. The pump and probe beams are set to overlap spatially and temporally at the surface of the various thin films. The transmitted probe light from the samples is collected and focused on the broad-band detector for recording the time-resolved excitation-induced difference spectrum (ΔA). During the measurements, the various thin films are constantly moved using a two-stage sample holder such that a fresh sample is available for each laser shot as well as to prevent a potentially substantial laser-induced heating effect on the films. The experiments were conducted at room temperature.

RESULTS AND DISCUSSION

The fundamental features of the samples in terms of the classified diffusion of the metal ions and respective oxides into the host TiO_2 layer were explored in detail. The core observation is that the dopant agents are mainly metal ions in the host ionic crystal of TiO_2. Here, we fully characterized the prepared Co-doped TiO_2 thin films by TEM and EELS; previously, they were investigated by X-ray diffraction (XRD) and Raman spectroscopy techniques.[27] The TEM image clearly confirms the preserved multilayer structures of the thin films even after the annealing process, with four layers of TiO_2 and three layers of the respective metals well-defined and clearly distinguishable, as presented in Figure 1A. The inset high-resolution TEM (HRTEM) image shows that the TiO_2 layers are partially crystallized, agreeing well with previous XRD and Raman results.[27]

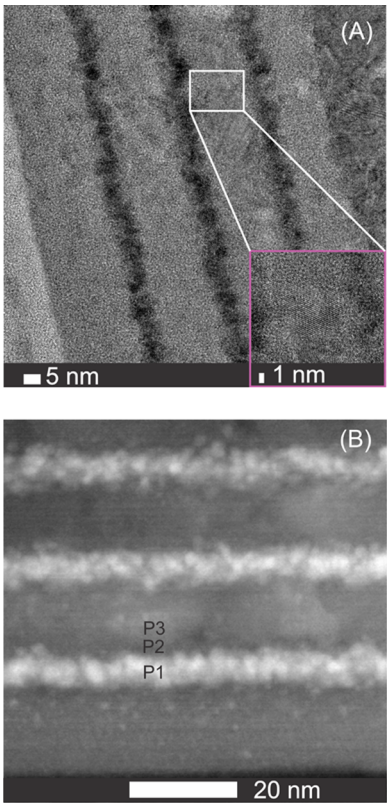

Figure 1. HRTEM image of a Co/TiO_2-30s film (A). STEM image of a Co/TiO_2-30s film (B). P1 refers to the position in the metal layer, and P2 and P3 refer to the positions at the edge and center of the TiO_2 layer, respectively. EELS spectra were taken at positions P1−P3 for analysis of the distribution of Co in the multilayer thin films.

In addition, we used EELS scans of a cross section (Figure 1B) of the samples to investigate the actual diffused concentration of the metal ions into the TiO_2 layer. The obtained EELS spectra were acquired from the metal layer to the center of the TiO_2 layer, as indicated in Figure 1 by positions P1 (the metal layer) and P2 and P3 (both in the TiO_2 layer). In the Co/TiO_2 (ions and oxides) films, we found that the amount of Co ions diffused into the TiO_2 layer (P3) was relatively substantial. In addition, the significant relative difference in the elementary ratio of Co/(Co + Ti) between Co/TiO_2-10s and Co/TiO_2-30s is mainly apparent in the Co layer at 26.923% and 66.019%, respectively (Table 1). At positions P2 and P3, there is a remarkable decrease in these respective values compared with the case of the initial

Table 1. Co/(Co + Ti) Elementary Ratios (%) in Co/TiO_2-10s and Co/TiO_2-30s Thin Films

	Co/(Co + Ti) ratio		
sample	P1	P2	P3
Co/TiO_2-10s	26.923	5.000	2.299
Co/TiO_2-30s	66.019	6.154	2.899

state (P1), but the actual percentages of diffused Co ions at P3 are 2.299% and 2.899%, confirming that Co was dispersed into the TiO_2 layers. This is consistent with the TA data (see below).

Apparently, the exact concentration of Co and W dopant atoms involved a large inaccuracy, but, on the other hand, there was no clear signature to predict the possibility of the appearance of cobalt oxides and tungsten oxides in the actual layers of Co/TiO_2-10s and W/TiO_2-10s. The reason might be due to the relatively high amount of titanium effectively suppressing the crystallization of cobalt oxides especially in Co/TiO_2-10s. Direct evidence of the presence of cobalt oxides and tungsten oxides in Co/TiO_2-10s and W/TiO_2-10s was not observed in either the XRD or Raman spectroscopy experiments. However, we cannot exclude the possibility that the associated oxides were partially diffused into the layers of Co/TiO_2-30s and W/TiO_2-30s because of the actual relatively high percentage of Co and W in the respective metal layers. However, if we assumed that a small fraction of Co or W is present as metal oxides, this will not add appreciable uncertainty to the measured ultrafast carrier dynamics because these oxides will have their own band gap rather than creating electron trapping states in the band gap of TiO_2, which is responsible for quenching of the excited carrier.

The elementary ratio of Co/(Co + Ti) in the TiO_2 layer is approximately below 7%, as indicated in Table 1, in good agreement with Griffin and Chambers et al.,[30,31] who claimed that the maximum dopant concentration of Co ions associated with TiO_2 films can reach 10%. Nevertheless, more Co ions are contained in the TiO_2 configuration of Co/TiO_2-30s compared with the case of Co/TiO_2-10s. This observation was confirmed by our ultrafast spectroscopy results (see below).

The surface analysis demonstrated that Co and W ions indeed diffused into the TiO_2 layer and served as dopant agents, which subsequently caused modification of the electronic band structure. In addition, the respective oxides and O ions were incorporated alongside the atoms in the TiO_2 layer. It is appropriate to clarify that a small percentage of the atoms were dispersed into the TiO_2 layer despite the fact that the distribution was inhomogeneous, as suggested by the TEM and EELS scans. Spatial compositional variations were clearly present, and the deviations were pronounced, but the atoms and metal ions were both present in this regime. It is worth pointing out that the inhomogeneity of the metal distribution did not affect the measured dynamics because we performed our TA experiment in a transmission mode and the measured signal reflected the average dynamics of the excited area.

In this section, the obtained results from steady-state and ultrafast TA spectroscopy are discussed. In Figure 2, we present the steady-state absorption spectra of the undoped TiO_2 (A) and doped TiO_2−Co−TiO_2 (B) and TiO_2−W−TiO_2 (C) films with the wavelength ranging from 300 to 1500 nm. The absorption edges of the TiO_2−M−TiO_2 multilayer thin films are red-shifted compared with the fundamental absorption edge, which is ascribed to the dopant metals that effectively cause a change in the band-gap energy of the TiO_2 thin films. In other words, this observation indicates that the band structure of TiO_2 is modified

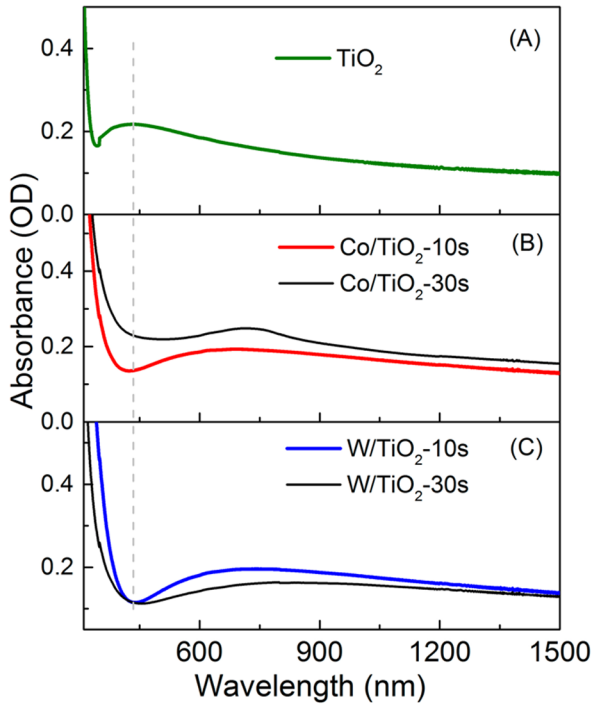

Figure 2. Steady-state absorption spectra of a TiO_2 film (A), Co/TiO_2-10s and Co/TiO_2-30s films (B), and W/TiO_2-10s and W/TiO_2-30s films (C). The TiO_2-M-TiO_2 multilayer thin films are red-shifted compared with the nondoped TiO_2 films, indicating that the band structure of the semiconductor oxide is modified significantly by metal doping.

significantly by metal doping. This red shift of the TiO_2 spectrum can be attributed to doping with ions of low electrical negativity because this mechanism is associated with the ability of an atom to attract the electron density toward itself.[32] In addition, very often, a shift in the band-gap transitions toward longer wavelengths is observed in the doped layers,[33] in good agreement with our observation. It is worth mentioning that the band gap of a TiO_2 polycrystalline thin film can be varied from 3.5 to 3.0 eV with tail down to the visible spectral range. This depends on postdeposition annealing, lattice constants, the grain size, the morphology, defects including oxygen ones, and the annealing temperature.[34−38]

fs-TA information was collected using an Ultrafast Systems Helios UV−NIR spectrometer integrated with a Ti:sapphire femtosecond regenerative amplifier operating at 800 nm with 35 fs pulses and a repetition rate of 1 kHz. A description of the experimental setup is given in Figure 3. The TA spectra obtained by probing with white light in the UV−vis range after 350 nm excitation are shown in Figure 4 for the case of undoped TiO_2 and 30 s deposition time for W- and Co-doped TiO_2. The probed data display clear excited states for decay times ranging from −0.7 to +103 ps for the 30 s deposition time. The pronounced effect indicates that the transient spectra strongly depend on the doping deposition time. The consistency of red shift as in the steady-state spectrum is clearly demonstrated throughout the displayed data. Utilizing a global-fitting procedure, we report our major findings in terms of the characteristics of the trapped carrier states in Figure 5. Figure 5A shows the carrier recombination of the undoped and Co-doped TiO_2 films. As can be clearly seen, the carrier dynamics of the undoped TiO_2 is much slower than that of the doped ones, indicating that the measured ultrafast carrier dynamics are associated with carrier

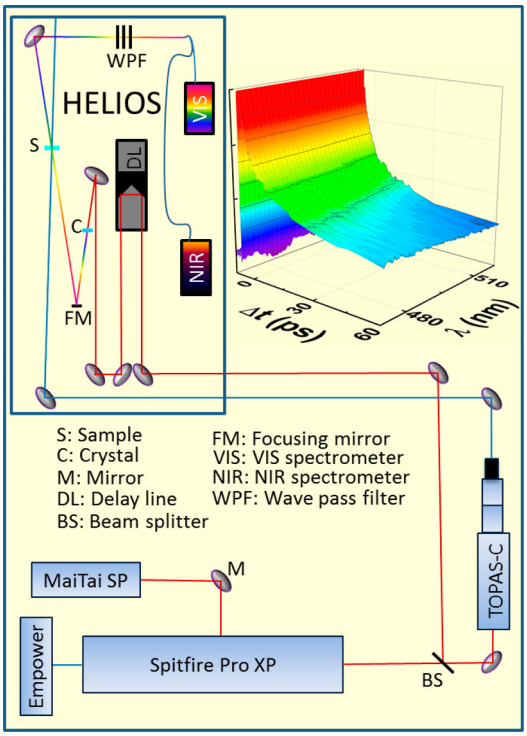

Figure 3. Experimental setup of fs-TA spectroscopy showing integration of the ultrafast Helios UV−NIR spectrometers with both a Spitfire Pro 35F-XP regenerative amplifier and a TOPAS-C two-stage parametric amplifier.

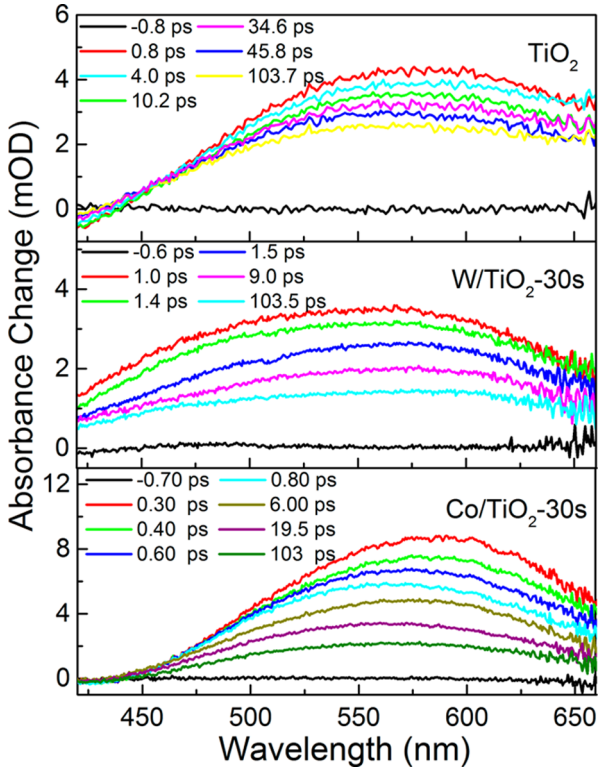

Figure 4. Average TA spectra of a TiO_2 (A), W/TiO_2-30s (B), and Co/TiO_2-30s (C) films at different time delays and an excitation of 350 nm.

trapping to the defect states created in the TiO_2 band gap by metal doping. Each decay curve has a fast component associated with a time constant of about 2−8 ps and a slow component with

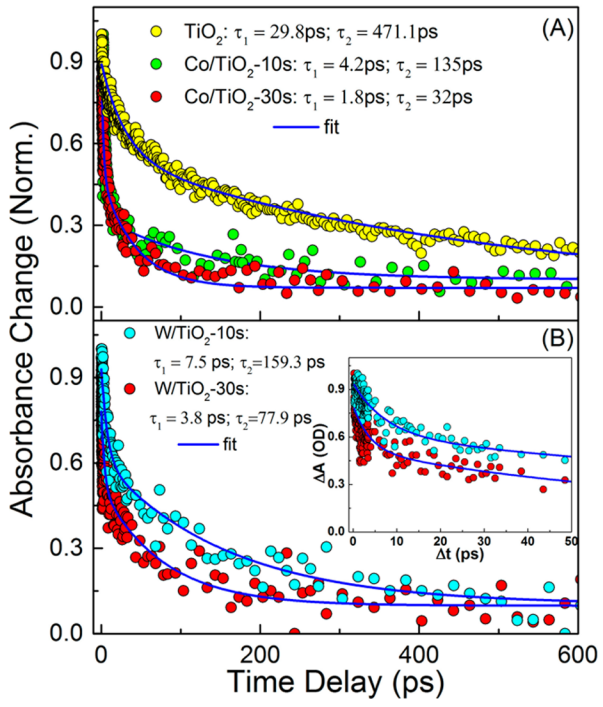

Figure 5. Comparison of the different doping concentration effects on the kinetics: (A) TiO_2, Co/TiO_2-10s, and Co/TiO_2-30s films; (B) W/TiO_2-10s and W/TiO_2-30s films. The kinetics are extracted at 578 nm, and the broad-band probe pulse is in the spectral range of 340−700 nm. A global-fitting procedure for the carrier trapping indicates a significant effect of the doping concentration.

a time constant of 40−160 ps. More precisely, in the Co/TiO_2-10s system, two different time components are found with values of $\tau_1 = 4.2 \pm 0.40$ ps and $\tau_2 = 135 \pm 12.0$ ps. In the case of Co/TiO_2-30s, the time components are $\tau_1 = 1.8 \pm 0.35$ ps and $\tau_2 = 32 \pm 2.7$ ps. Analogously, the time components for W/TiO_2-10s are $\tau_1 = 7.5 \pm 0.85$ ps and $\tau_2 = 159.3 \pm 15.0$ ps, and for W/TiO_2-30s, they are $\tau_1 = 3.8 \pm 0.65$ ps and $\tau_2 = 77.9 \pm 7.6$ ps. It should be noted that the carrier trapping is estimated by fitting the kinetic data with a two-exponential decay function: $\Delta A = A_1 \exp(-t/\tau_1) + A_2 \exp(-t/\tau_2)$, where A_i and τ_i, $i = 1$ and 2, are the time-independent coefficients and time constants determined by the excitation fluence. As can be seen, the carrier trapping of W/TiO_2-30s is almost a factor of 2 slower compared with that for Co/TiO_2-30s. The determined time components are associated with fast and slow times, respectively. The former one is linked to the decay of the electron to the defect state located below the CB. Similarly, the second time component is attributed to electrons decaying to the deep-level trapping state allocated between the VB and CB, near the center of the band gap. These findings associated with the concentration gradient are consistent with the literature,[39] indicating that, as the generated defect states are shifted (closer to the CB edge), the doping concentration is increased, eventually providing a faster trapping time.

A similar result was observed for other doped semiconductor materials.[6,16,24−26,40,41] In these cases, the slow component is also attributed to carrier trapping in the deep-level energy states, which can attract electrons from the CB or holes from the VB. Essentially, the time constants of both the fast and slow components progressively decrease with increasing doping concentration. Similarities are obtained in W-doped TiO_2 films (as shown in Figure 5B). Figure 5 further reveals that the values of the carrier lifetime in the doped TiO_2 films significantly

dx.doi.org/10.1021/am5026159 | ACS Appl. Mater. Interfaces 2014, 6, 10022−10027

depend on the dopant metals. Comparing the carrier lifetime of Co/TiO_2-10s in Figure 5A with that of W/TiO_2-10s in Figure 5B, we observe that the value of Co/TiO_2-10s is almost a factor of 2 faster than that of W/TiO_2-10s. Similarities are also observed in the carrier lifetimes of Co/TiO_2-30s and W/TiO_2-30s. The drift in the time of carrier trapping caused by the dopant mass effect is explained by the creation of additional defect states or different distributions of the defect levels in the band gap.[39,42]

Variations in the pump fluence and the concentration effects studied here suggest different behaviors. Whereas the former has no substantial effect on the carrier dynamics, the latter has a pronounced effect on reduction of the carrier lifetime. Additionally, Co is a promising candidate as a dopant agent because it provides a relatively faster trapping time compared with W, which, in turn, has a larger mass. More specifically, Figure 6A shows the kinetics of Co/TiO_2-10s under low (5.3 mJ/cm^2) and high (11.5 mJ/cm^2) pump fluence conditions. As can be seen, the kinetics are relatively comparable in both cases and do not display any significant differences, suggesting that the observed dynamics reflect only carrier trapping and completely exclude any heat contribution to the measured signal. The contribution from lattice heating is considerable, but an increase in the fluence by a factor of 2 has no significant effect on the kinetics. The photogenerated carrier density is expressed by the following equation: $N = j_p\alpha$, where j_p is the pump fluence (photons/cm^2) and α is the absorption coefficient of TiO_2 at the associated pump wavelength. The value of $\alpha = 0.23 \times 10^5$ cm^{-1} is determined from the measured absorbance (OD = 0.184) at the pump wavelength and the thickness (l = 80 nm) of the TiO_2 thin-film sample. The spot size of the laser beam is 440 μm; thus, N is calculated to be 2.13×10^{20} cm^{-3}. Figure 6B shows the kinetics of Co/TiO_2-30s under different excitation conditions at 350 and 475 nm. The lifetime of the trapped states of Co/TiO_2-30s at 350 nm excitation (Figure 6B) is slower than the one at 475 nm excitation. This can be associated with the mechanism whereby a higher excitation energy will inject electrons at an intrinsic energy level above the CB edge. Therefore, the electronic wavepacket undergoes intraband transitions in the CB, resulting in the fast component as the lifetime becomes slower and decays further to the defect level. In other words, the fast decay is slower at 350 nm excitation because the decay is convolved together with a growth due to intra-CB cooling.

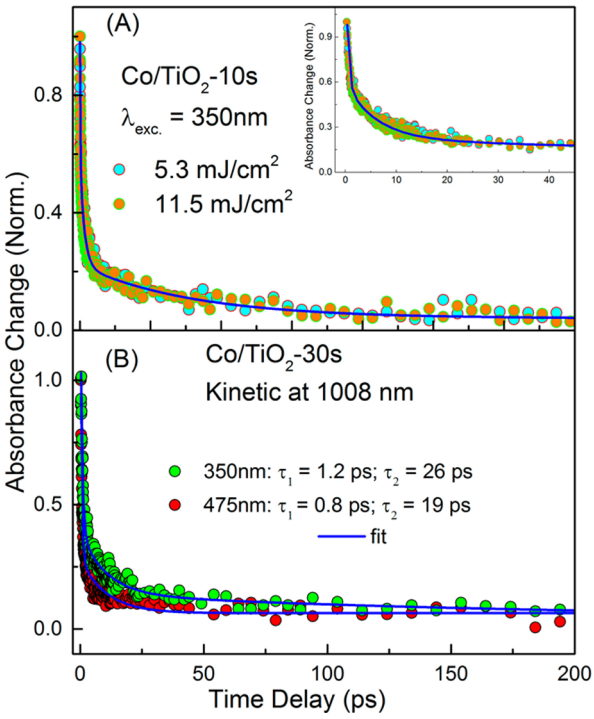

Figure 6. (A) Kinetics of a Co/TiO_2-10s film under different pump fluences, clearly indicating that the observed dynamics reflect only carrier trapping and completely exclude any contribution of heat to the measured signal. (B) Kinetics of a Co/TiO_2-30s film under different excitation conditions.

CONCLUSION

In summary, the ultrafast carrier dynamics has been examined for the first time for W/TiO_2-10s and -30s and Co/TiO_2-10s and -30s using broad-band TA spectroscopy with 120 fs temporal resolution. The observation of fast and slow time components was reported for each sample. These time components were attributed to the associated decay of the electronic wavepacket to the defect state near the CB and the deep-level trapping state, respectively. The obtained values for the time components are typically on the order of 2−8 ps for the fast one and analogously around 40−160 ps for the slow one, demonstrating the pronounced vital impact of the doping deposition time on the carrier trapping. In addition, our steady-state spectroscopy and imaging and fs-TA data demonstrate clearly that Co and W are present in the TiO_2 layer as metal ions rather than oxides. Our results may have implications for applications in electronic devices requiring ultrafast carrier recombination through trapped states. We further anticipate that our findings might serve as motivation for further investigation of the ultrafast carrier trapping dynamics in other semiconductor materials.

AUTHOR INFORMATION

Corresponding Author

*Phone: +966128084491; E-mail: omar.abdelsaboor@kaust.edu.sa.

Notes

The authors declare no competing financial interest.

ACKNOWLEDGMENTS

The work reported here was supported by King Abdullah University of Science and Technology.

REFERENCES

(1) Asahi, R.; Taga, Y.; Mannstadt, W.; Freeman, A. J. Electronic and Optical Properties of Anatase TiO_2. *Phys. Rev. B* **2000**, *61*, 7459−7465.

(2) Etgar, L.; Gao, P.; Xue, Z.; Peng, Q.; Chandiran, A. K.; Liu, B.; Nazeeruddin, M. K.; Grätzel, M. Mesoscopic $CH_3NH_3PbI_3/TiO_2$ Heterojunction Solar Cells. *J. Am. Chem. Soc.* **2012**, *134*, 17396−17399.

(3) Lee, S.; Lee, Y.; Kim, D. H.; Moon, J. Carbon-Deposited TiO_2 3D Inverse Opal Photocatalysis: Visible-Light Photocatalytic Activity and Enhanced Activity in a Viscous Solution. *ACS Appl. Mater. Interfaces* **2013**, *5*, 12526−12532.

(4) Paulauskas, I. E.; Modeshia, D. R.; Ali, T. T.; El-Mossalamy, E. H.; Obaid, A. Y.; Basahel, S. N.; Al-Ghamdi, A. A.; Sartain, F. K. Photocatalytic Activity of Doped and Undoped Titanium Dioxide Nanoparticles Synthesised by Flame Spray Pyrolysis. *Plat. Met. Rev.* **2013**, *57*, 32−43.

(5) Sun, M.; Zhu, D.; Ji, W.; Jing, P.; Wang, X.; Xiang, W. Exploring the Effect of Band Alignment and Surfaces States on Photoinduced Electron Transfer from $CuInS_2$/CdS Core/Shell Quantum Dots to TiO_2 Electrodes. *ACS Appl. Mater. Interfaces* **2013**, *5*, 12681−12688.

(6) Wang, X.; Chen, J. Q.; Barman, A. R.; Dhar, S.; Xu, Q.-H.; Venkatesan, T. Ariando Static and Ultrafast Dynamics of Defects of $SrTiO_3$ in $LaAlO_3/SrTiO_3$ Heterostructures. *Appl. Phys. Lett.* **2011**, *98*, 081916.
(7) Zaleska, A. Doped-TiO_2: A Review. *Recent Pat. Eng.* **2008**, *2*, 157−164.
(8) Chen, H.; Nanayakkara, C. E.; Grassian, V. H. Titanium Dioxide Photocatalysis in Atmospheric Chemistry. *Chem. Rev.* **2012**, *112*, 5919−5948.
(9) Park, M.-H.; Li, J.-H.; Kumar, A.; Li, G.; Yang, Y. Doping of the Metal Oxide Nanostructure and its Influence in Organic Electronics. *Adv. Funct. Mater.* **2009**, *19*, 1241−1246.
(10) Sardar, S.; Sarkar, S.; Myint, M. T. Z.; Al-Harti, S.; Dutta, J.; Pal, S. K. Role of Central Metal Ions in Hematoporphyrin Functionalized Titania in Solar Energy Conversion Dynamics. *Phys. Chem. Chem. Phys.* **2013**, *15*, 18562−18570.
(11) Bickley, R. I.; Gonzalez-Carreno, T.; Lee, J. S.; Palmisano, L.; Tilley, R. J. D. A Structural Investigation of Titanium Dioxide Photocatalysts. *J. Solid State Chem.* **1991**, *92*, 178−190.
(12) Fujishima, A.; Honda, K. Electrochemical Photolysis of Water at a Semiconductor Electrode. *Nature* **1972**, *238*, 37−38.
(13) Graetzel, M. Photoelectrochemical Cells. *Nature* **2001**, *414*, 338−344.
(14) Chen, X.; Mao, S. S. Titanium Dioxide Nanomaterials: Synthesis, Properties, Modifications, and Applications. *Chem. Rev.* **2007**, *107*, 2891−2959.
(15) Berger, T.; Sterrer, M.; Diwald, O.; Knözinger, E.; Panayotov, D.; Thompson, T. L.; Yates, J. T. J. Light-Induced Charge Separation in Anatase TiO_2 Particles. *J. Phys. Chem. B* **2005**, *109*, 6061−6068.
(16) Kang, J. U.; Frankel, M. Y.; Huang, J. W.; Kuech, T. F. Ultrafast Carrier Trapping in Oxygen-Doped Metal−Organic Vapor Phase Epitaxy GaAs. *Appl. Phys. Lett.* **1997**, *70*, 1560−1562.
(17) Auston, D. H. Impulse-Response of Photoconductors in Transmission-Lines. *IEEE J. Quantum Electron.* **1983**, *19*, 639−648.
(18) Valdmanis, J. A.; Mourou, G. Subpicosecond Electrooptic Sampling—Principles and Applications. *IEEE J. Quantum Electron.* **1986**, *22*, 69−78.
(19) Berera, R.; Grondelle, R. v.; Kennis, J. T. M. Ultrafast Transient Absorption Spectroscopy: Principles and Application to Photosynthetic Systems. *Photosynth. Res.* **2009**, *101*, 105−118.
(20) Klimov, V. I. Optical Nonlinearities and Ultrafast Carrier Dynamics in Semiconductor Nanocrystals. *J. Phys. Chem. B* **2000**, *104*, 6112−6123.
(21) Villamaina, D.; Bhosale, S. V.; Langford, S. J.; Vauthey, E. Excited-State Dynamics of Porphyrin−Naphthalenediimide−Porphyrin Triads. *Phys. Chem. Chem. Phys.* **2013**, *15*, 1177−1187.
(22) Wang, H.; Saxena, C.; Quan, D.; Sancar, A.; Zhong, D. Femtosecond Dynamics of Flavin Cofactor in DNA Photolyase: Radical Reduction, Local Solvation and Charge Recombination. *J. Phys. Chem. B* **2005**, *109*, 1329−1333.
(23) Zhang, L.; Kao, Y.-T.; Qi, W.; Wang, L.; Zhong, D. Femtosecond Studies of Tryptophan Fluorescence Dynamics in Proteins: Local Solvation and Electronic Quenching. *J. Phys. Chem. B* **2006**, *110*, 18097−18103.
(24) Yamada, Y.; Yasuda, H.; Tayagaki, T.; Kanemitsu, Y. Photocarrier Recombination Dynamics in Highly Excited $SrTiO_3$ Studied by Transient Absorption and Photoluminescence Spectroscopy. *Appl. Phys. Lett.* **2009**, *95*, 121112.
(25) Taguchi, S.; Tayagaki, T.; Kanemitsu, Y. Luminescence and Magnetic Properties of Co Doped ZnO Nanocrystals. *IOP Conf. Ser.: Mater. Sci. Eng.* **2009**, *6*, 012029.
(26) Maity, P.; Debnath, T.; Akbar, A.; Verma, S.; Ghosh, H. N. Ultrafast Electron-Transfer and -Trapping Dynamics in the Inter-Band-Gap States of ZrO_2 Nanoparticles Sensitized by Baicalein. *J. Phys. Chem. C* **2013**, *117*, 17531−15539.
(27) Yang, Y.; Zhang, Q.; Zhang, B.; Mib, W. B.; Chen, L.; Lia, L.; Zhao, C.; Diallo, E. M.; Zhang, X. X. The Influence of Metal Interlayers on the Structural and Optical Properties of Nano-Crystalline TiO_2 Films. *Appl. Surf. Sci.* **2012**, *258*, 4532−4537.
(28) Sun, J.; Yu, W.; Usman, A.; Isimjan, T. T.; Dgobbo, S.; Alarousu, E.; Takanabe, K.; Mohammed, O. F. Generation of Multiple Excitons in Ag_2S Quantum Dots: Single High-Energy versus Multiple-Photon Excitation. *J. Phys. Chem. Lett.* **2014**, *5*, 659−665.
(29) El-Ballouli, A. a. O.; Alarousu, E.; Bernardi, M.; Aly, S. M.; Lagrow, A. P.; Bakr, O. M.; Mohammed, O. F. Quantum Confinement-Tunable Ultrafast Charge Transfer at the PbS Quantum Dot and Phenyl-C61-butyric Acid Methyl Ester Interface. *J. Am. Chem. Soc.* **2014**, *136*, 6952−6959.
(30) Chambers, S. A.; Thevuthasan, S.; Farrow, R. F. C.; Marks, R. F.; Thiele, J. U.; Folks, L.; Samant, M. G.; Kellock, A. J.; Ruzycki, N.; Ederer, D. L.; Diebold, U. Epitaxial Growth and Properties of Ferromagnetic Co-Doped TiO_2 Anatase. *Appl. Phys. Lett.* **2001**, *79*, 3467−3469.
(31) Griffin, K. A.; Varela, M.; Pennycook, S. J.; Pakhomov, A. B.; Krishnan, K. M. Atomic-Scale Studies of Cobalt Distribution in Co−TiO_2 Anatase Thin Films: Processing, Microstructure, and the Origin of Ferromagnetism. *J. Appl. Phys.* **2006**, *99*, 08M114.
(32) Lu, L.; Xia, X.; Luo, J. K.; Shao, G. Mn-Doped TiO_2 Thin Films with Significantly Improved Optical and Electrical Properties. *J. Phys. D: Appl. Phys.* **2012**, *45*, 485102.
(33) Kment, S.; Kmentova, H.; Kluson, P.; Krysa, J.; Hubicka, Z.; Cirkva, V.; Gregora, I.; Solcova, O.; Jastrabik, L. Notes on the Photo-Induced Characteristics of Transition Metal-Doped and Undoped Titanium Dioxide Thin Films. *J. Colloid Interface Sci.* **2010**, *348*, 198−205.
(34) Gao, Y.; Masuda, Y.; Peng, Z.; Yonezawa, T.; Koumoto, K. Room Temperature Deposition of a TiO_2 Thin Film From Aqueous Peroxotitanate Solution. *J. Mater. Chem.* **2003**, *13*, 608−613.
(35) Li, G. H.; Yang, L.; Jin, Y. X.; Zhang, L. D. Structural and Optical Properties of TiO_2 Thin Film and TiO_2 + 2 wt.% $ZnFe_2O_4$ Composite Film Prepared by r.f. Sputtering. *Thin Solid Films* **2000**, *368*, 163−167.
(36) Choudhury, B.; Dey, M.; Choudhury, A. Shallow and Deep Trap Emission and Luminescence Quenching of TiO_2 Nanoparticles on Cu Doping. *Appl. Nanosci.* **2014**, *4*, 499−506.
(37) Wunderlich, W.; Miao, L.; Tanemura, M.; Jin, P.; Kaneko, K.; Terai, A.; Nabatova-Cabin, N.; Belkada, R. Ab-initio Calculations of the Optical Band Gap of TiO_2 Thin Films. *Int. J. Nanosci.* **2004**, *3*, 439−445.
(38) Tatlıdil, I.; Bacaksızb, E.; Burukc, C. K.; Breend, C.; Sökmena, M. A Short Literature Survey on Iron and Cobalt Ion Doped TiO_2 Thin Films and Photocatalytic Activity of These Films Against Fungi. *J. Alloys Compd.* **2012**, *517*, 80−86.
(39) Meier, D. L.; Hwang, J. M.; Campbell, R. B. The Effect of Doping Density and Injection Level on Minority-Carrier Lifetime as Applied to Bifacial Dendritic Web Silicon Sorlar-Cells. *IEEE Trans. Electron Devices* **1988**, *35*, 70−79.
(40) Yamada, Y.; Kanemitsu, Y. Blue Photoluminescence of Highly Photoexcited Rutile TiO_2: Nearly Degenerate Conduction-band Effects. *Phys. Rev. B* **2010**, *82*, 113103.
(41) Yamada, Y.; Kanemitsu, Y. Determination of Electron and Hole Lifetimes of Rutile and Anatase TiO_2 Single Crystals. *Appl. Phys. Lett.* **2012**, *101*, 133907.
(42) Dhaka, V. D. S.; Tkachenko, N. V.; Lemmetyinen, H.; Pavelescu, E. M.; Guina, M.; Tukiainen, A.; Konttinen, J.; Pessa, M.; Arstila, K.; Keinonen, J.; Nordlund, K. Effects of Heavy-Ion and Light-Ion Irradiation on the Room Temperature Carrier Dynamics of InGaAs/GaAs Quantum Wells. *Semicond. Sci. Technol.* **2006**, *21*, 661−664.